Electronic Supplementary Material (ESI) for RSC Advances.

Supporting Information

Construction of A Conjugated Covalent Organic Framework for Iodine Capture

Chao Gao†, Xuhui Guan†, Lei Chen, Haoran Hu, Lei Shi, Chong Zhang, Chengguo Sun, Yang Du, Bingcheng Hu*

School of Chemical Engineering, Nanjing University of Science and Technology, Nanjing 210094, PR China

Section S1. Materials and Methods

All reagents and solvents were purchased from commercial sources and Nanjing university of science and technology drug depot without further purification. 1,2,4,5-tetrakis-(4-formylphenyl)benzene (TPB-CHO) were synthesized according to the literature [S1], 2,3,5,6-tetramethyl-*p*-phenylenediamine (TMPD) was purchased without further purification. ^{1}H and ^{13}C NMR spectra were measured on a Bruker AVANCE III 500 M spectrometer. Solid-state NMR spectra were recorded at ambient temperature on a Bruker AVANCE III 400M spectrometer. Fourier transform infrared (FT-IR) spectra were recorded on a Nicolet iS10 FTIR Spectrometer. Powder X-ray diffraction (PXRD) patterns were obtained on a Bruker-AXS D8 Advance with Cu Kα line (λ = 1.5418 Å). Thermogravimetric analysis (TGA) from 50-800 °C was carried out on a STA 449 F5 Jupiter in nitrogen atmosphere using a 10 °C/min ramp without equilibration delay. The nitrogen isotherms were measured at 77 K using an Autosorb-iQ (Quantachrome) surface area size analyzer. Before measurement, the samples were degassed in vacuum at 120 °C for 12 h.

Stability test. TPB-TMPD-COF (20 mg) were kept for 24 h at room temperature in water, acetone, DMF, hexane and NaOH (0.1 M), respectively. The samples were collected by filtration and rinsed with, THF and $CHCl_3$ for several times. The COFs samples were dried and subjected to PXRD analysis.

General procedure for iodine vapor sorption. An open small vial (3 mL) containing the COF sample (~50 mg) was placed in a large vial (50 mL) containing iodine (4 g). The large vial was sealed and kept in an oven at 77 °C. After a certain period, the large vial was cooled to room temperature. The small vial containing the

COF sample was weighted and placed back into the iodine-containing large vial. The large vial was sealed and put back in the oven at 77 °C to continue the adsorption till the mass of the small vial containing the COF sample did not change.

General procedure for recycling the COF samples. The iodine-captured COF sample was added to MeOH (20 mL) in a vial at 25 °C, and MeOH was refreshed every 2 h until no color of the solution was observed. The COF sample was collected by filtration, washed with MeOH, dried under vacuum at 120 °C overnight and reused for the next cycle.

Procedure for iodine escape investigation. An open vial (10 mL) containing the iodine-loaded COF sample was placed in room temperature. After a certain period, the vial containing the COF sample was weighted. The investigation was carried for a period of 5 days.

Section S2. Chemical Synthesis

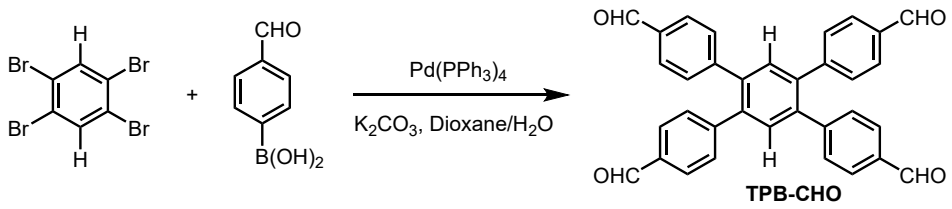

Figure S1. Synthesis of **TPB-CHO**.

Synthesis of 1,2,4,5-tetrakis-(4-formylphenyl)benzene (TPB-CHO): It was synthesized according to the literature[S1]. 1,2,4,5-Tetrabromobenzene (3.0 g, 7.6 mmol), 4-formylphenylboronic acid (6.8 g, 45.5 mmol), palladium tetrakis(triphenylphosphine) (0.9 g, 0.76 mmol), and potassium carbonate (8.4 g, 60.8 mmol) were added to a flask containing 1,4-Dioxane/H_2O (150 mL/15 mL). The mixture was heated under nitrogen at 90 °C for 3 days. After cooling to room temperature, the solvent was removed under reduced pressure. Then the residues were dissolved in CH_2Cl_2, washed with water and brine, dried over anhydrous Na_2SO_4. After that, the solvent was evaporated under reduced pressure and the crude product was purified by column chromatography to yield **TPB-CHO** as a white solid. ^{1}H NMR (500

MHz, $CDCl_3$, ppm): δ = 10.00 (s, 4H), 7.80 (d, *J* = 7.0 Hz, 8H), 7.60 (s, 2H), 7.39 (d, *J* = 6.9 Hz, 8H). ^{13}C NMR (125 MHz, $CDCl_3$, ppm): δ= 191.76, 146.15, 139.59, 135.19, 132.88, 130.49, 129.77.

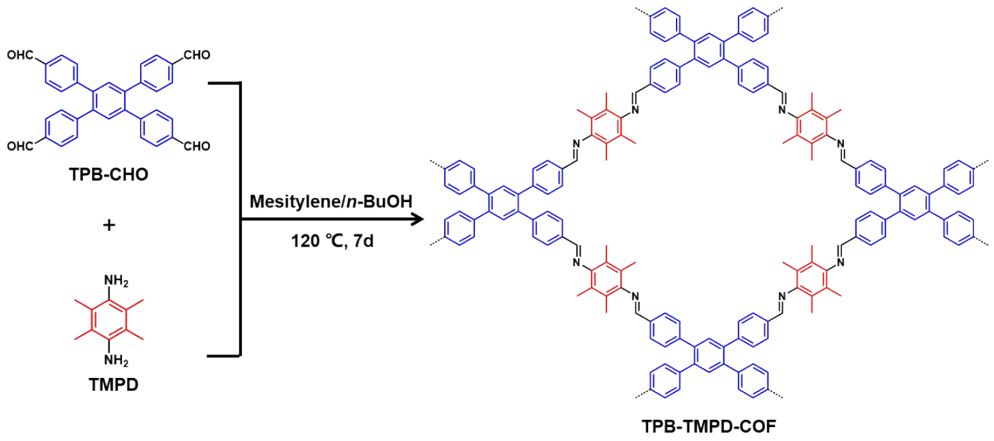

Figure S2. Synthesis of **TPB-TMPD-COF**.

Synthesis of TPB-TMPD-COF. A Pyrex tube was charged with TPB-CHO (59.4 mg, 0.12 mmol), TMPD (39.4 mg, 0.24 mmol), mesitylene (3.5 mL), *n*-butanol (1.5 mL) and 6 M aqueous acetic acid (0.6 mL). After being degassed by freeze-pump-thaw technique for three times and then sealed under vacuum, the tube was placed in an oven at 120 °C for 7 d. The resulting precipitate was filtered, exhaustively washed by Soxhlet extractions with tetrahydrofuran and chloroform for 2 d, dried at 80 °C under vacuum for 12 h. The TPB-TMPD-COF was isolated as yellow-green powder (66 mg, yield 73%).

Section S3. Structure Simulation

The unit cell structures of the eclipsed AA and staggered AB stacking modes were calculated using the density-functional tight-binding method including Lennard-Jones dispersion (DFTB-D), as implemented in the DFTB+ program package. DFTB is an approximate density functional theory method based on the tight binding approach and utilizes an optimized minimal LCAO Slater-type all-valence basis set in combination with a two-center approximation for Hamiltonian matrix elements. The Coulombic interaction between partial atomic charges was determined using the self-consistent

charge (SCC) formalism. Lennard-Jones type dispersion was employed in all calculations to describe van der Waals and π-stacking interactions. The lattice dimensions were optimized simultaneously with the geometry. The standard DFTB parameters for X–Y element pairs (X, Y = C, H, O and N) interactions were selected from the mio-1-1 set.

The TPB-TMPD-COF models were generated using Materials Studio suite of programs. Vertex positions were obtained from the Reticular Chemistry Structure Resource.[S2] Firstly, the eclipsed model was built and the symmetry of lattice was degraded to *P*1. Then the lattice model was fully optimized using the Forcite module. The staggered arrangement for TPB-TMPD-COF was also examined by offsetting the alternating stacked units from the eclipsed model. Pawley refinement was carried out using Reflex, a software package for crystal determination from XRD pattern. Unit cell dimension was set to the theoretical parameters. The Pawley refinement was performed to optimize the lattice parameters iteratively until the R_{wp} value converges and the overlay of the observed with refined profiles shows good agreement. The pseudo-Voigt profile function was used for whole profile fitting and Berrar–Baldinozzi function was used for asymmetry correction during the refinement processes. Line broadening from crystallite size and lattice strain were both considered.

Table S1. Fractional atomic coordinates for the unit cell of TPB-TMPD-COF with single-pore AA stacking structure.

TPB-TMPD-COF		Space Group: *P*-1 a = 4.1747 Å, b = 19.4152 Å, c = 20.0465 Å, α = 122.5978°, β = 63.9059°, and γ = 132.6397°,		
C1	C	0.51324	2.07002	2.00458
C2	C	0.50906	2.14356	2.01559
C3	C	0.4756	2.19986	2.08714
C4	C	0.46818	2.26853	2.09888
C5	C	0.4943	2.28225	2.03915

C6	C	0.52707	2.22686	1.96786
C7	C	0.53258	2.15833	1.95657
C8	C	0.487	2.35436	2.0518
C9	C	0.56056	3.01138	2.93489
C10	C	0.54388	2.94317	2.93206
C11	C	0.62848	3.01754	2.86362
C12	C	0.99423	3.08619	2.83673
C13	C	1.0483	3.094	2.77082
C14	C	0.73885	3.03286	2.73106
C15	C	0.37798	2.96246	2.75663
C16	C	0.32402	2.95473	2.82246
C17	C	0.79233	3.04534	2.66465
N18	N	0.50542	2.99266	2.62856
C19	C	0.51445	2.9984	2.56361
C20	C	0.83113	3.07127	2.53542
C21	C	0.81437	3.07195	2.47207
N22	N	0.50131	2.36691	1.99736
C23	C	0.49833	2.43481	2.00097
C24	C	0.48932	2.50097	2.0672
C25	C	0.49298	2.56558	2.06552
C26	C	0.50999	2.36345	1.86469
C27	C	0.52642	2.49594	1.86006
C28	C	-0.185	2.85077	2.42796
C29	C	-0.15033	2.85133	2.55818
H30	H	0.45404	2.18982	2.13669
H31	H	0.44079	2.31331	2.15724
H32	H	0.5494	2.23769	1.91873
H33	H	0.55661	2.1129	1.89839
H34	H	0.46855	2.4002	2.11007

H35	H	0.57734	2.89529	2.87652
H36	H	1.24852	3.13583	2.86864
H37	H	1.34511	3.15029	2.74939
H38	H	0.12757	2.91133	2.72363
H39	H	0.03103	2.89707	2.84287
H40	H	1.09011	3.10213	2.64398
H41	H	0.25281	2.29575	1.87337
H42	H	0.80306	2.37281	1.8495
H43	H	0.47635	2.36791	1.8182
H44	H	0.84587	2.52724	1.82847
H45	H	0.41577	2.53409	1.86983
H46	H	0.3296	2.42413	1.82654
H47	H	-0.09125	2.84094	2.36607
H48	H	-0.42189	2.86319	2.45176
H49	H	-0.31093	2.78887	2.4382
H50	H	-0.2563	2.87689	2.61936
H51	H	-0.04375	2.81344	2.55083
H52	H	-0.40615	2.80539	2.52732

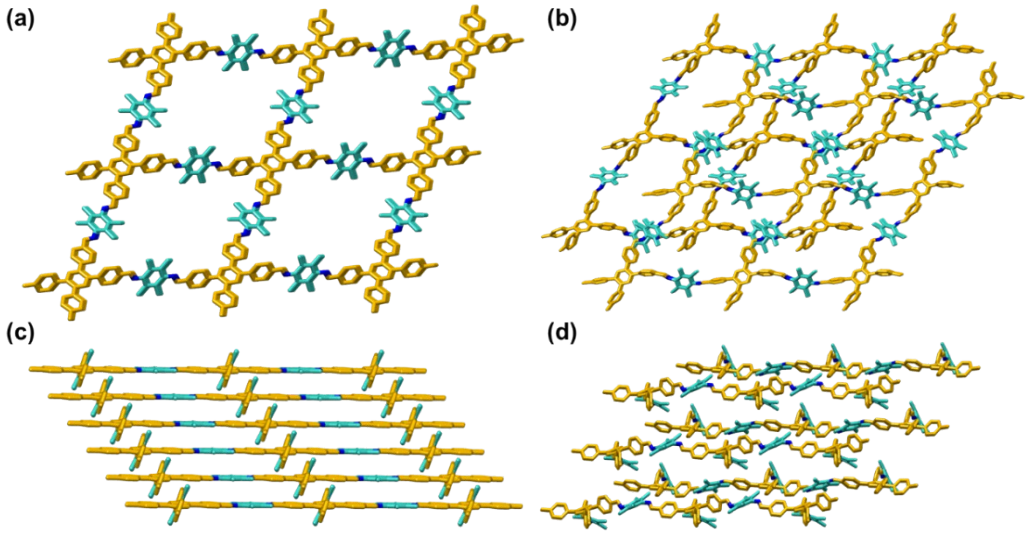

Figure S3. Simulated Structure of TPB-TMPD-COF with single-pore structure. (a) top view of AA stacking, (c) side view of AA stacking, (b) top view of AB stacking, (d)

side view of AB stacking.

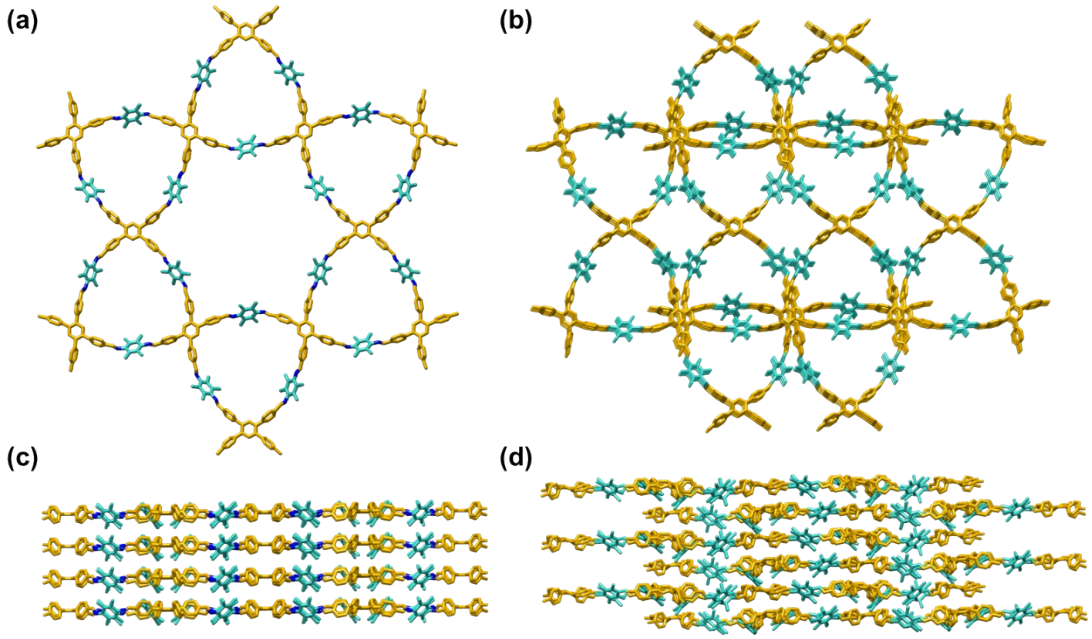

Figure S4. Simulated Structure of TPB-TMPD-COF with dual-pore structure. (a) top view of AA stacking, (c) side view of AA stacking, (b) top view of AB stacking, (d) side view of AB stacking.

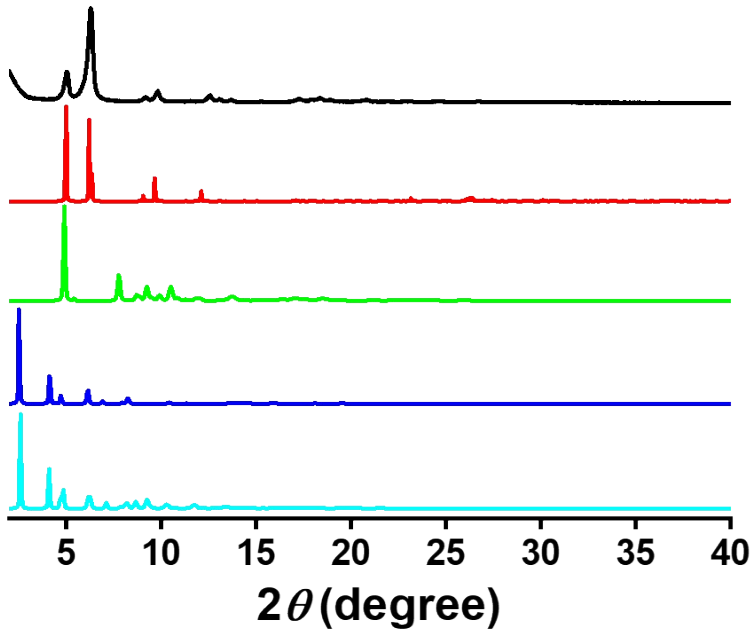

Figure S5. The experimental (black curve) and simulated PXRD patterns (red curve: AA stacking with single-pore structure; green curve: AB stacking with single-pore

structure; blue curve: AA stacking with dual-pore structure; cyan curve: AB stacking with dual-pore structure) of TPB-TMPD-COF.

Section S4. Characterization

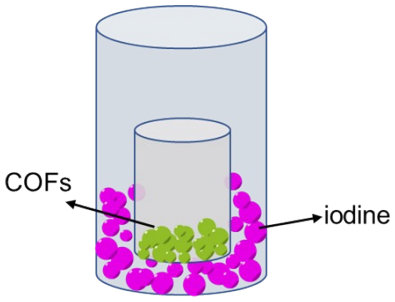

Figure S6. Schematic diagram of iodine vapor adsorption test by COFs.

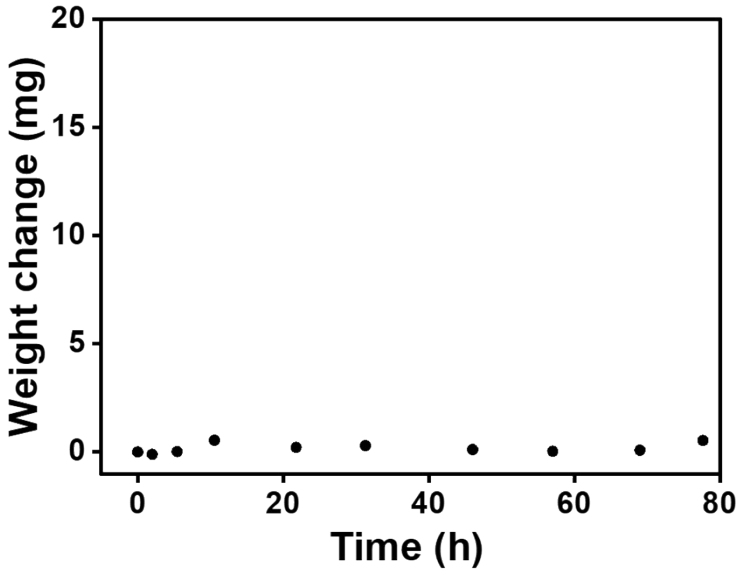

Figure S7. The blank control experiment: the weight change of the open small vial in the iodine vapor sorption experiment.

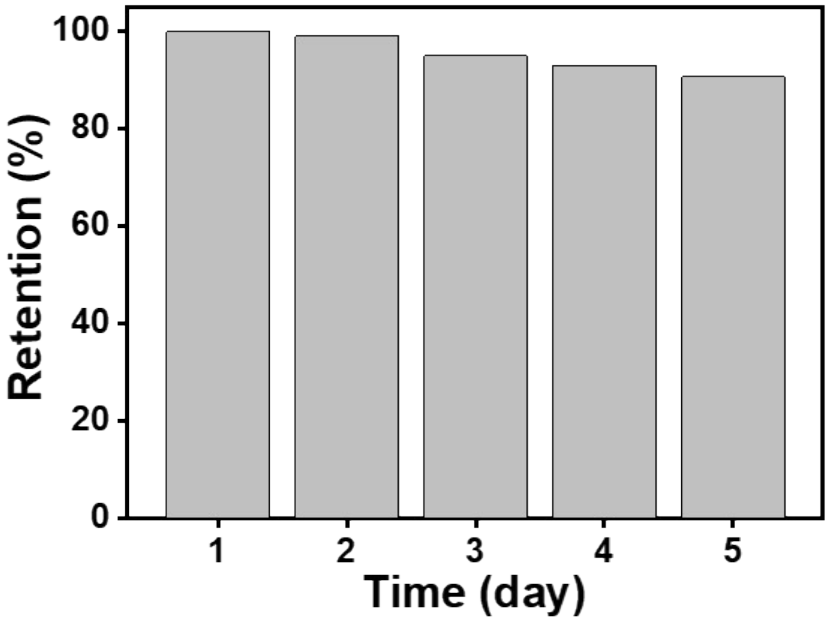

Figure S8. The blank control experiment: the weight change of the open small vial in the iodine vapor sorption experiment.

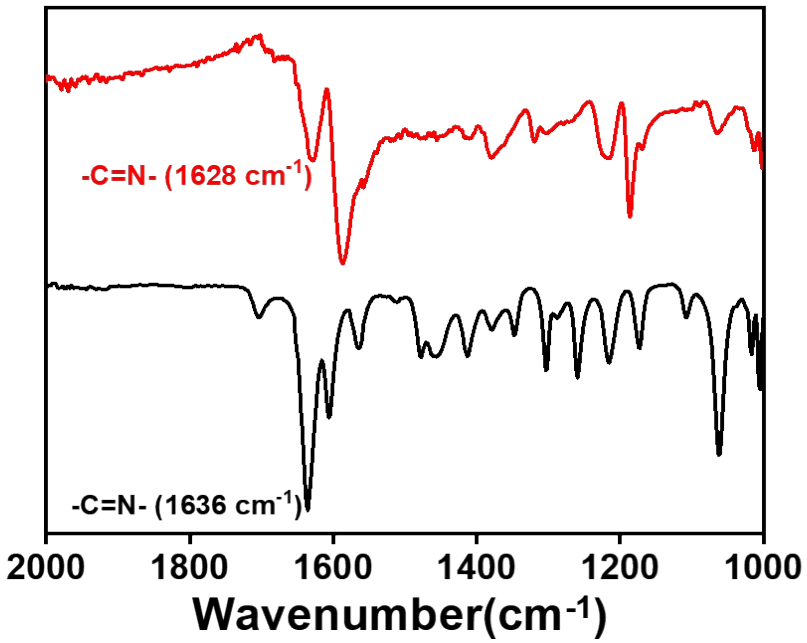

Figure S9. FT-IR spectra of TPB-TMPD-COF before (black curve) and after (red curve) iodine uptake.

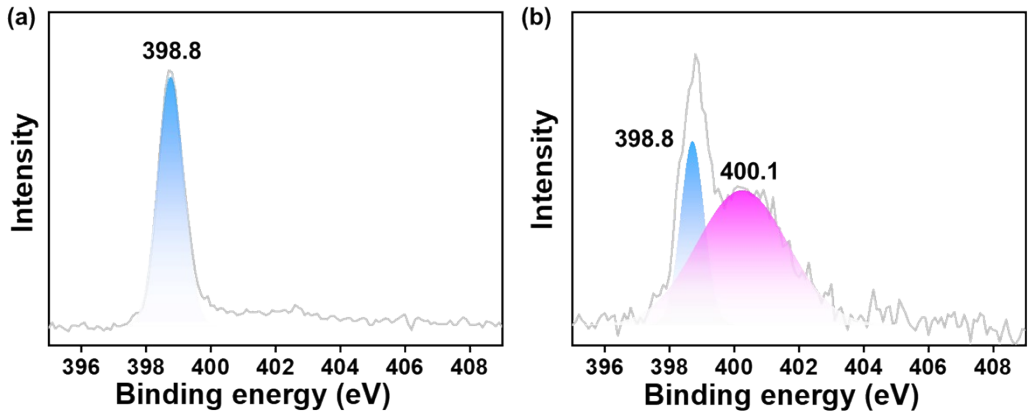

Figure S10. Comparison of XPS N 1s spectra of TPB-TMPD-COF (a) and iodine loaded TPB-TMPD-COF.

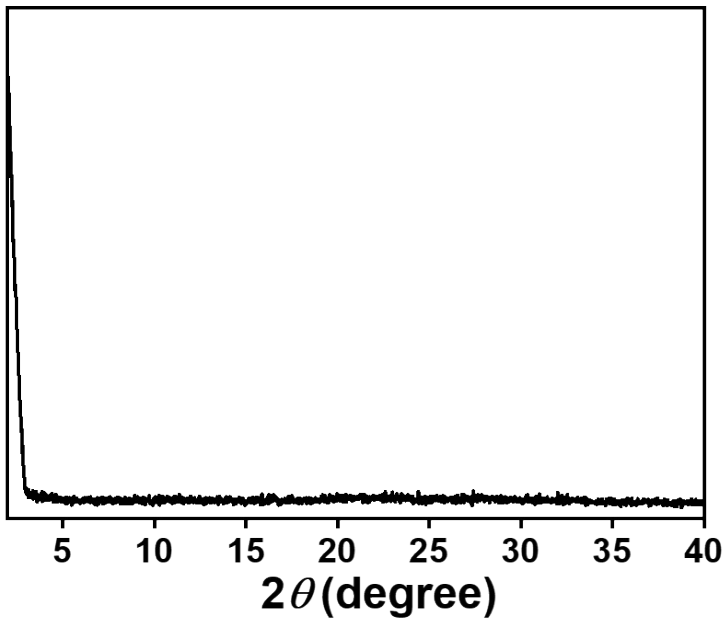

Figure S11. PXRD patterns of iodine-captured TPB-TMPD-COF.

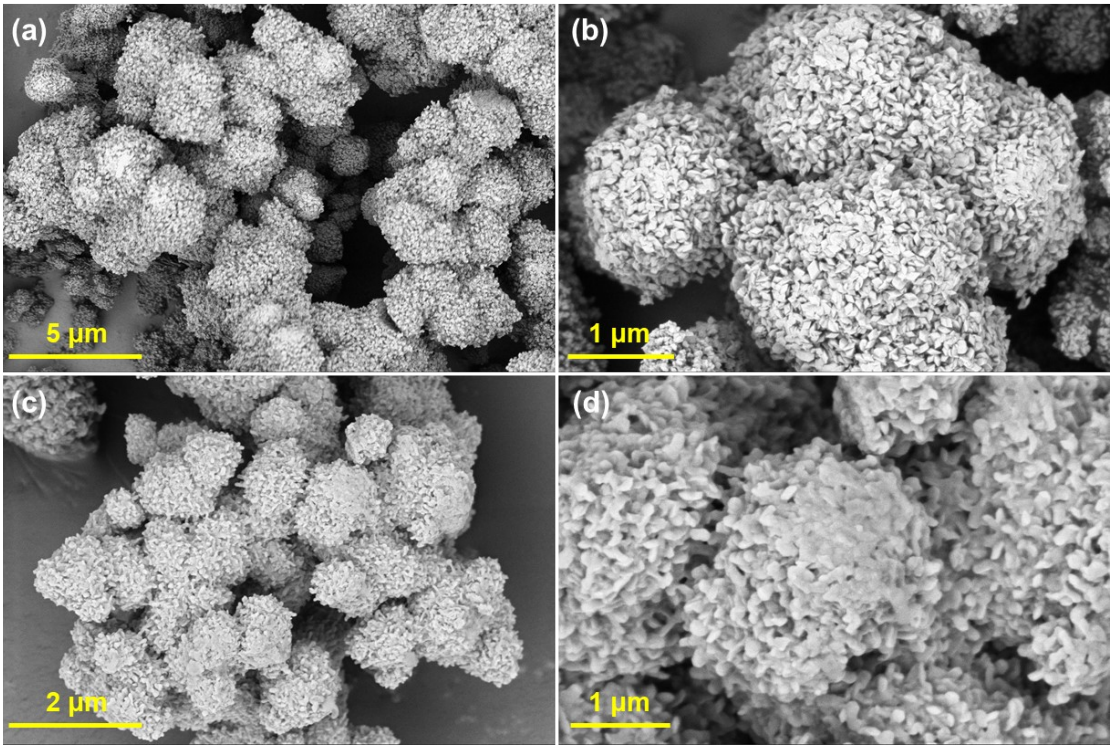

Figure S12. SEM image of TPB-TMPD-COF before (a, b) and after (c, d) iodine uptake.

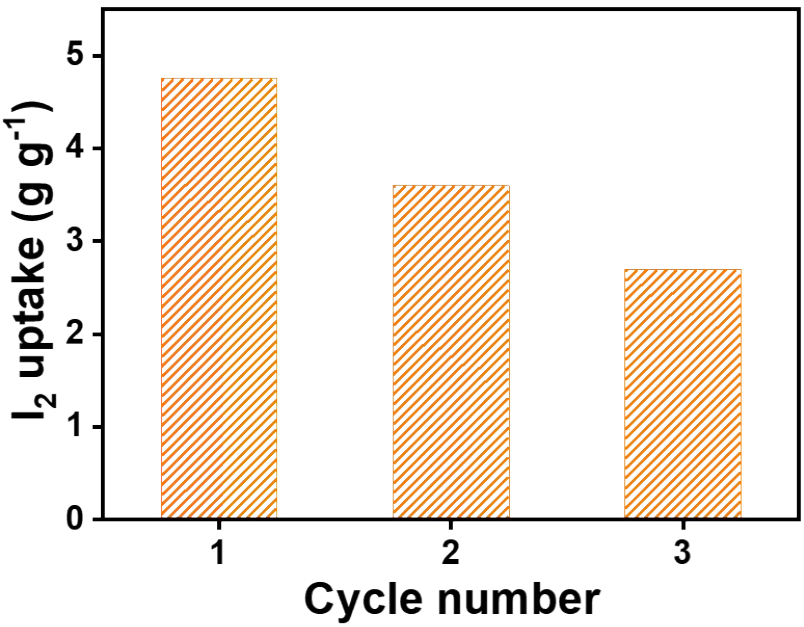

Figure S13. Iodine vapor capture cycle of TPB-TMPD-COF.

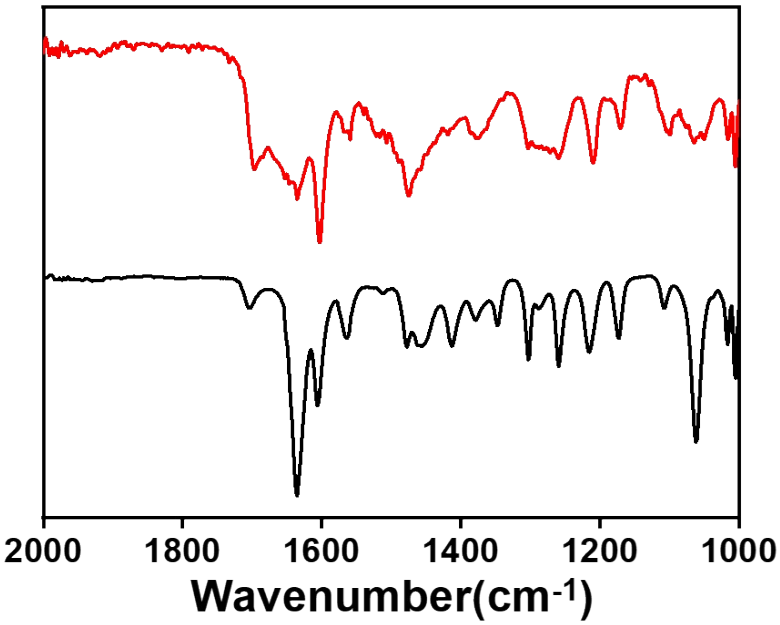

Figure S14. FT-IR spectra of TPB-TMPD-COF (black curve) and regenerated TPB-TMPD-COF (red curve) after three runs of iodine vapor capture and release.

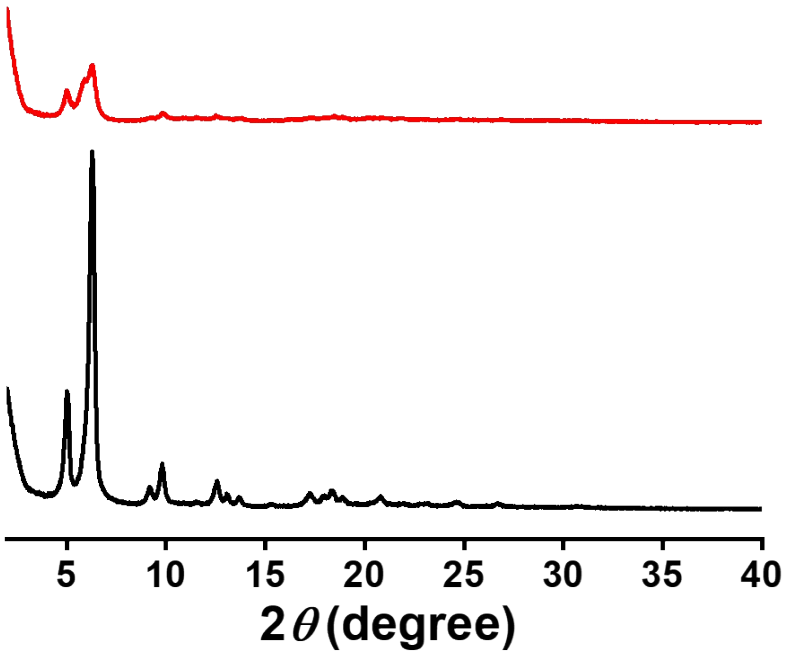

Figure S15. PXRD patterns of TPB-TMPD-COF (black curve) and regenerated TPB-TMPD-COF (red curve) after three runs of iodine vapor capture and release.

Table S2. Summary of iodine adsorption capacity for reported adsorbents.

Adsorbent	Temperature (℃)	I_2 uptake (g g^{-1})	Ref.
iCOF-AB-50	75	10.21	S3
COF-TAPT	75	8.61	S4
JUC-561	75	8.19	S5
COF-TAPB	75	7.94	S4
HOF-TAM-BPY	75	6.78	S6
TFB-DB COF	75	6.4	S7
QTD-COF-V	75	6.29	S8
TFB-BD COF	75	6.23	S7
TPB-DMTP COF	75	6.26	S9
SCU-COF-2	75	6.0	S10
TJNU-203	77	5.88	S11
H-COF	77	5.72	S12
TFPB-PyTTA-COF	77	5.6	S13
F-COF-2	77	5.51	S14
TPT-DHBD COF	75	5.4	S15
TJNU-204	77	5.33	S11
COF-LZU1	77	5.30	S16
QTD-COF-3	75	5.16	S8
TAPA-PDA COF	77	5.09	S17
TFB-Td COF	75	4.97	S7
DbTd-COF	75	4.93	S18
TFFPy-TMPD-COF	77	4.8	S19
PCMP-Y5	85	4.75	S20
TPB-TMPD-COF	77	4.75	**This work**
COF-DL229	75	4.7	S21
H-C-CTPs	75	4.6	S22
CMP-LS5	70	4.4	S23
Meso-COF-3	75	4.0	S24
IPN-CSU-1	75	3.57	S25

FcTz-POP	75	3.96	S26
TFBT-1	75	3.15	S27
PAF-24	75	2.76	S28
Uassis-PC800	77	2.25	S29
BN foam	77	2.12	S30
$[Cd_2(COO)_4N_4)]$	50	0.66	S31
Ag^+@Zeolite Mordenitres	95	0.28	S32
CMP-4	75	2.08	S33

References

S1. O'Keeffe, M. et al. The reticular chemistry structure resource (RCSR) database of, and symbols for, crystal nets. *Acc. Chem. Res.* **2008**, 41, 1782–1789.

S2. O'Keeffe, M. et al. The reticular chemistry structure resource (RCSR) database of, and symbols for, crystal nets. *Acc. Chem. Res.* **2008**, 41, 1782–1789.

S3. Xie, Y. et al. Ionic functionalization of multivariate covalent organic frameworks to achieve an exceptionally high iodine-capture capacity. *Angew. Chem. Int. Ed.* **2021**, *60*, 22432.

S4. Xie, Y. et al. Efficient and simultaneous capture of iodine and methyl iodide achieved by a covalent organic framework. *Nat. Commun.* **2022**, *13*, 2878.

S5. Chang, J. et al. Tetrathiafulvalene-based covalent organic frameworks for ultrahigh iodine capture. *Chem. Sci.*, **2021**, *12*, 8452−8457.

S6. Wang, Y.et al. Pore polarity engineering in hydrogen-bonded organic frameworks for enhanced iodine capture. *J. Mater. Chem. A*, **2022**, *10*, 18730–18736.

S7. Song, S. et al. Theoretical screening and experimental synthesis of ultrahigh-iodine capture covalent organic frameworks. *ACS Appl. Mater. Interfaces* **2021**, *13*, 10513–10523.

S8. Guo, X. et al. Colyliform crystalline 2D covalent organic frameworks (COFs) with quasi-3D topologies for rapid I_2 adsorption. *Angew. Chem. Int. Ed.*, **2020**, *59*, 22697–22705.

S9. Wang, P. et al. Exceptional iodine capture in 2D covalent organic frameworks. *Adv. Mater.* **2018**, *30*, 1801991.

S10. He, L. et al. A nitrogen-rich covalent organic framework for simultaneous dynamic capture of iodine and methyl iodide. *Chem*, **2021**, *7*, 699−714.

S11. Zhang, L. et al. High iodine uptake in two-dimensional covalent organic frameworks. *Chem. Commun.,* **2021***, 57,* 5558.

S12. Zhang, Y. et al. Linkage design in two-dimensional covalent organic frameworks for high iodine uptake. *Macromol. Rapid Commun.* **2023**, 2200787.

S13. Zhou, M. et al. Highly conjugated two-dimensional covalent organic frameworks for efficient iodine uptake. *Chem Asian J.* **2022**, *17*, e202200358.

S14. Zhang, Y. et al. Covalent organic frameworks constructed from flexible building blocks: high porosity, crystallinity, and iodine uptake. *CrystEngComm*, **2023**, *25*, 525–529.

S15. Guo, X. et al. Mechanistic insight into hydrogen-bond-controlled crystallinity and adsorption property of covalent organic frameworks from flexible building blocks. *Chem. Mater.* **2018**, *30*, 2299–2308.

S16. Yang, Y. et al. Insight into volatile iodine uptake properties of covalent organic frameworks with different conjugated structures. *Solid State Chem.*, **2019**, *279*, 120979.

S17. Chen, R. et al. Synthesis of nitrogen-containing covalent organic framework with reversible iodine capture capability. *Microporous Mesoporous Mater.*, **2021**, *312*, 110739.

S18. Wu, Z. et al. Adsorption of iodine on adamantane-based covalent organic

frameworks. *ChemistrySelect*, **2021**, *6*, 10141–10148.

S19. Gao, C. et al. Enhancing the iodine adsorption capacity of pyrene-based covalent organic frameworks by regulating the pore environment. *Macromol. Rapid Commun*. **2023**, 2300311.

S20. Zuo, H. et al. High-yield synthesis of pyridyl conjugated microporous polymer networks with large surface areas: from molecular iodine capture to metal-free heterogeneous catalysis. *Macromol. Rapid Commun.*, **2020**, *41*, 2000489.

S21. Wang, C. A 3D covalent organic framework with exceptionally high iodine capture capability. *Chem.-Eur. J.*, **2018**, *24*, 585.

S22. Xu, Y. et al. Room-temperature synthesis of hollow carbazole-based covalent triazine polymers with multiactive sites for efficient iodine capture-catalysis cascade application. *Acs Applied Polymer Materials*, **2020**, *2*, 3704.

S23. Wang, S. et al. Ultrahigh volatile iodine capture by conjugated microporous polymer based on *N,N,N′,N′*-tetraphenyl-1,4-phenylenediamine. *Polym. Chem.*, **2019**, *10*, 2608.

S24. An, S. et al. Porosity modulation in two-dimensional covalent organic frameworks leads to enhanced iodine adsorption performance. *Ind. Eng. Chem. Res.*, **2019**, 58, 10495.

S25. Ai, C. et al. Enhanced iodine capture by incorporating anionic phosphate unit into porous networks. *Sep. Purif. Technol.* **2021**, *279*, 119799.

S26. Wang, Y. et al. Ferrocene-based porous organic polymers for high-affinity iodine capture. *Chem. Eng. J.* **2020**, *380*, 122420.

S27. Li, H. et al. Effective iodine adsorption by nitrogen-rich nanoporous covalent organic frameworks. *ACS Appl. Nano Mater.* **2023**, *6*, 1295.

S28. Yan, Z. et al. Highly efficient enrichment of volatile iodine by charged porous aromatic frameworks with three sorption sites. *Angew. Chem. Int. Ed.*, **2015**, *54*,

12733.

S29. Xiao, K. et al. Excellent performance of porous carbon from urea-assisted hydrochar of orange peel for toluene and iodine adsorption. *Chem. Eng. J.*, **2020**, *382*, 122997.

S30. Li, G. et al. Effective capture and reversible storage of iodine using foam-like adsorbents consisting of porous boron nitride microfibers. *Chem. Eng. J.*, **2020**, *382*, 122833.

S31. Shi, B.-B. et al. A rigid and porous metal-organic frameworks with 1D rhombus channels and double walls: selective adsorption of CO_2 over N_2, iodine capture, and fluorescence. *Inorg. Chem. Commun.*, **2019**, *102*, 147.

S32. Chapman, K. W. et al. Radioactive iodine capture in silver-containing mordenites through nanoscale silver iodide formation. *J. Am. Chem. Soc.*, **2010**, *132*, 8897.

S33. Dai, D. et al. Macrocyclic arenes-based conjugated macrocycle polymers for highly selective CO_2 capture and iodine adsorption. *Angew. Chem. Int. Ed.*, **2021**, *60*, 8967−8975.